九州大学大学院総合理工学府報告
第 37 巻 第 2 号 1-5 頁 平成 28 年 2 月

Engineering Sciences Reports, Kyushu University
Vol. 37, No. 2, pp. 1-5, FEB, 2016

Structural analysis of mesoporous ZrO_2 and TiO_2 nanofiber mats prepared by electrospinning methods

Chanmin LEE[*1] Yong-Gun SHUL[*2] and Hisahiro EINAGA[*3,†]
[†]E-mail of corresponding author: einaga.hisahiro.399@m.kyushu-u.ac.jp

(Received December 29, 2015, accepted January 9, 2016)

Ag particles loaded mesoporous zirconia oxide (ZrO_2) and titanium oxide (TiO_2) nanofibers were prepared by electrospinning methods followed by calcination at 500-600ºC. The crystal structure of the Ag particles were investigated by X-ray diffraction (XRD) and scanning electron microscopy (SEM). The fiber diameters for the ZrO_2 and TiO_2 mats were in the range of 60-160 nm and 50-450 nm, respectively. X-ray line broadening analysis showed that they were composed of smaller sized crystallites. Nitrogen-adsorption studies revealed that the ZrO_2 and TiO_2 fibers have both mesoporous and macroporous structures, which were originated from the aggregation of smaller crystallites than the fiber diameters and the interspaces formed by randomly oriented nanofibers. The deposition of Ag on the fibers followed by calcination at 500ºC changed the distribution of the mesopore sizes.

Key words: *ZrO_2, TiO_2, mesoporous materials, electrospinning method*

1. Introduction

Zirconium dioxide (ZrO_2) and titanium dioxide (TiO_2) are widely used in the catalysts for supporting materials because they are chemically and physically stable and have generally high surface areas. These materials are generally prepared by liquid-phase and gas-phase synthesis processes[1,2]. As for the catalyst supports, mesoporous materials which have the pores whose diameters are in the range of 2-50 nm because they generally have large surface areas and intrinsic properties caused by the porous structures. Over the decades, mesoporous materials have been developed using liquid-phase preparation methods using surfactants as the template molecules[3]. The preparation of mesoporous ZrO_2 and TiO_2 has been reported by several groups and the efficacy of these materials for catalytic reactions has been discussed[4,5]. In addition, much attention has been recently focused on the metal oxides that have macroporous structures because the catalyst properties also depended on the shape and morphologies of the catalysts. For instance, the control of the catalyst shape and structures improved the oxidation of diesel soot emitted from the diesel engines. Therefore, the fabrication of metal oxides having macropores is one of the important targets in the research area of catalysis science.

The electrospinning phenomenon was firstly observed by Rayleigh in 1897. Since then, this has been utilized for fabricating polymeric and inorganic fibrous materials[6-8], due to their convenient and versatile method. In particular, electrospun ceramic fibers are often in the spotlight due to the outstanding characteristics such as high surface area and hierarchical pore[9,10]. Additionally, they are widely used in a wide variety of applications, for example, as filtration membranes[11], delivery of bioactive agents[12], batteries or solar cells[13,14], proton exchange membrane fuel cells[15] and catalytic reaction[16].

We herein report that the ZrO_2 and TiO_2 nanofibers which have both mesoporous and macroporous structures have been successfully prepared by the electrosppining method. The characteristic porous and crystallographic structure of ZrO_2 and TiO_2 nanofibers are

*1 Department of Molecular and Material Sciences
*2 Department of Chemical and Biomolecular Engineering, Yonsei University
*3 Department of Energy and Material Sciences

investigated by scanning electron microscopy (SEM), N_2 adsorption desorption isotherm, Barrett-Joyner-Halenda (BJH) pore size distribution and X-ray diffraction (XRD) analyses. We also investigated the effect of Ag loading on the porous structures of ZrO_2 and TiO_2 fibers because supported silver catalysts draw much attention due to their potential application for solid-solid heterogeneous catalytic reactions such as catalytic soot oxidation and catalytic sterilization.

2. Experimental

2. 1. Chemicals and preparation of ZrO_2 and TiO_2 nano-fibrous support and catalysts

Zirconium oxychloride ($ZrOCl_2 \cdot 8H_2O$) and Titanium isopropoxide were purchased from Kishida Chemical. Silver nitrate ($AgNO_3$, 99.8%) and N, N-dimethylformamide (DMF, 99.5%) were obtained from Wako Pure Chem Ind Ltd. Polyvinylpyrrolidone (PVP, MW= 1.3×106) were obtained from Sigma–Aldrich Japan.

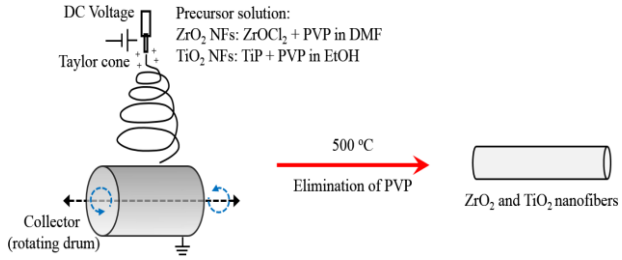

Fig. 1. Schematic illustration of ZrO_2 and TiO_2 nanofibers synthesis sequence.

Figure 1 shows the schematic illustration of ZrO_2 and TiO_2 nanofibers synthesis sequence. To prepare ZrO_2 nanofiber, we used a general electropinning method followed by a heat treatment. 3g of $ZrOCl_2 \cdot 8H_2O$ and 1g of PVP were dissolved in 9g DMF. Then, this precursor mixture was vigorously stirred at room temperature for 6 h. The prepared precursor solution was electronspun onto a rotating drum with a distance between the drum surface and spinneret tip of 12 cm. High voltage of 18 kV was applied at the stainless steel needle (27 G, inner diameter = 0.21 mm) and feeding rate was maintained at 0.5 mL h^{-1}. The electrospun Zr/PVP nanofibers were calcined at 600°C for 3 hrs under the air atmosphere to perfectly eliminate PVP.

For the synthesis of TiO_2 fibers, 0.73 g of PVP and 0.35 g Acetic acid were dissolved in 7 g EtOH. Then, 1.8 g Titanium isopropoxide was added to the prepared solution, and this mixture vigorously stirred at room temperature for 30 min. The electrospinning of TiO_2 fiber was performed with the prepared precursor solution at a voltage of 14 kV and distance between the collector (rotating drum) and syringe needle (30 G, inner diameter = 0.15 mm) of 15 cm. During electro-spinning, a feeding rate and humidity were kept at 0.6 mL hr-1 and 30 % RH, respectively. To remove the polymer substance (PVP) and form the pure TiO_2 fiber, the electrospun TiO_2/PVP fibers were calcined at 500°C for 6 hrs in air atmosphere.

5 wt% silver was loaded on the calcined ZrO_2 and TiO_2 fibers by the following procedures; (1) calculated amount of $AgNO_3$ (5 wt% Ag) was dissolved in 100 mL of pure water; (2) 0.1 g of fibers were added to solution; (3) to evaporate water and decompose the metal salts, they were stirred at 250°C for 3 h; (4) finally the sample was calcined at 500°C for 5 h.

2. 2. Characterization

The morphologies of ZrO_2 and TiO_2 nanofibers were observed by the scanning electron microscopy (SEM; JEOL). X-ray diffraction were performed by means of RINT 2000 (RIGAKU) recorded from 25 to 100 ° with scan speed of 10 min^{-1}. The Brunauer-Emmett-Teller (BET) surface area and pore diameter were analyzed by nitrogen sorption at 77 K (BELSORP II; BEL). To discuss the chemical condition on the surface of the catalyst, X-ray photoelectron spectroscopy (XPS; Thermo VG Scientific, UK) was conducted using a monochromated Al X-ray source (Al kα line at 1486.6 eV) at X-ray power of 36 W under a vacuum (7.8×10^{-9} mbar).

3. Results and discussion

3. 1. Structural properties of ZrO_2 nanofibers

The shapes and morphological structures were investigated using a scanning electron microscopy (SEM). Figure 2 displays SEM images and fiber diameter distribution of eletrospun ZrO_2 nanofibers. The ZrO_2 nanofibers exhibited an average diameter of 105 nm (selected 200 samples) with range of about 60 to160 nm and a rough surface morphology, as shown in Fig. 2a. Figure 2c also shows that the ZrO_2 nanofiber mats have the porous structures, which were composed of the

randomly oriented ZrO_2 fibers. The interspace sizes are in the range of 1-20 μm.

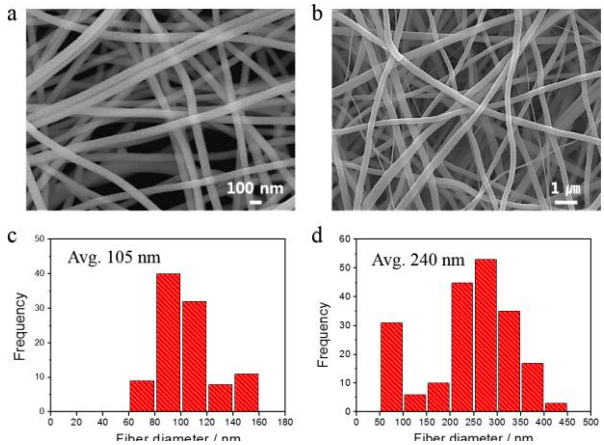

Fig. 2. SEM images of electrospun nanofibers (a) ZrO_2 and (b) TiO_2 and fiber diameter distribution of (c) ZrO_2 and (d) TiO_2 nanofibers.

Figure 3a exhibits the XRD patterns of ZrO_2, which confirms the crystal structure. The major diffraction peaks corresponding to (11$\bar{1}$), (111), (002), (110), (21$\bar{1}$), (220), (131), (311) and (400) of crystalline monoclinic structure (JCPDS No. 74-0815) and (101), (110), (112), (211), (202) and (220) of crystalline tetragonal phase (JCPDS No. 79-0815) were clearly

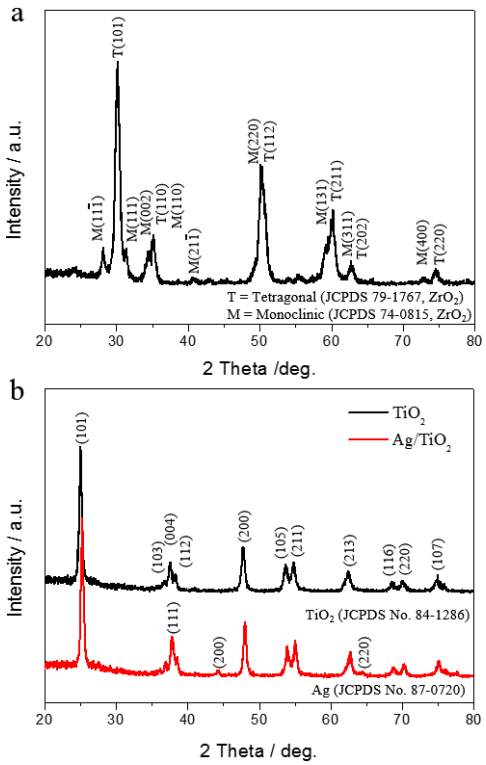

Fig. 3. XRD patterns of (a) ZrO_2 and (b) TiO_2 and Ag supported TiO_2 nanofiber.

observed, respectively. According to peak band width, line-broadening analyses were carried out to estimate the crystalline sizes of the ZrO_2 fibers using the Scherrer equation (1).

$$D = 0.94\lambda / (\beta 1/2 \cos\theta) \qquad (1)$$

Where D is the crystallite size, λ is the X-ray wavelength of 1.54056 Å, β1/2 is the full width at half maximum (FWHM) of (101) peak and θ is the Bragg angle. The average size of the ZrO_2 crystallines thus determined were 12 nm, which was much smaller than that of the ZrO_2 fibers determined by the SEM images. This findings indicates that the fibers were composed of the aggregated crystallites of monoclinic and tetragonal phases.

The pore structure of ZrO_2 and Ag/ZrO_2 nanofibers was investigated by nitrogen adsorption studies. Figure 4 shows the nitrogen adsorption-desorption isotherms obtained at 77 K (Fig. 4a and b). ZrO_2 and Ag/ZrO_2 nanofibers showed type III isotherms and H3 hysteresis loops, which are the characteristics of N_2 adsorption-desorption on mesoporous materials. Moreover, pore size distribution measured from Barrett, Joyner and Halenda (BJH) method exhibited the maximum peaks in range of 4.63 – 7.98 nm, further confirming that the ZrO_2 fibers have mesoporous structures (see Fig. 5a).

Figure 4 also shows the N_2 adsorption -desorption isotherms for Ag deposited ZrO_2 (Ag/ZrO_2) nanofibers. The material has also exhibit the hysteresis loop in the relative pressure range of 0.6-0.9. The pore size distribution obtained by the BJH method shows that the Ag/ZrO_2 nanofibers have the pores in the range of 2-20 nm with a maximum at 10 nm. Thu, the pore sizes distribution was slightly changed after deposition of $AgNO_3$ on the ZrO_2 fibers followed by the calcination.

BET surface areas of ZrO_2 and Ag/ZrO_2 nanofibers were calculated to be 15.5, and 9.5 $m^2\ g^{-1}$, respectively. Because the Ag loading was 5wt%, the decrement of the BET surface area by Ag deposition cannot be explained in terms of the decrement of the ZrO_2 content. It is likely that the sintering of ZrO_2 in the calcination process gave rise to the decrease in ZrO_2 surface area.

3. 2. Structural properties of TiO_2 fibers

Figure 2 shows the SEM images of the TiO_2 nanofibers prepared by the electrospinning method. After calcination at 500◦C, the

diameter of TiO_2 nanofiber ranged from about 50 to 450 nm (average diameter of 240 nm) and exhibited a rough surface morphology (Fig. 2b and d). The sizes are much larger than those for ZrO_2 fibers. The difference is presumably due to the combustion of polymathic substance (PVP) at high temperature. Figure 2 also shows that the TiO_2 nanofiber mats have the porous structures, which were composed of the randomly oriented TiO_2 fibers, as in the case of ZrO_2 fibers.

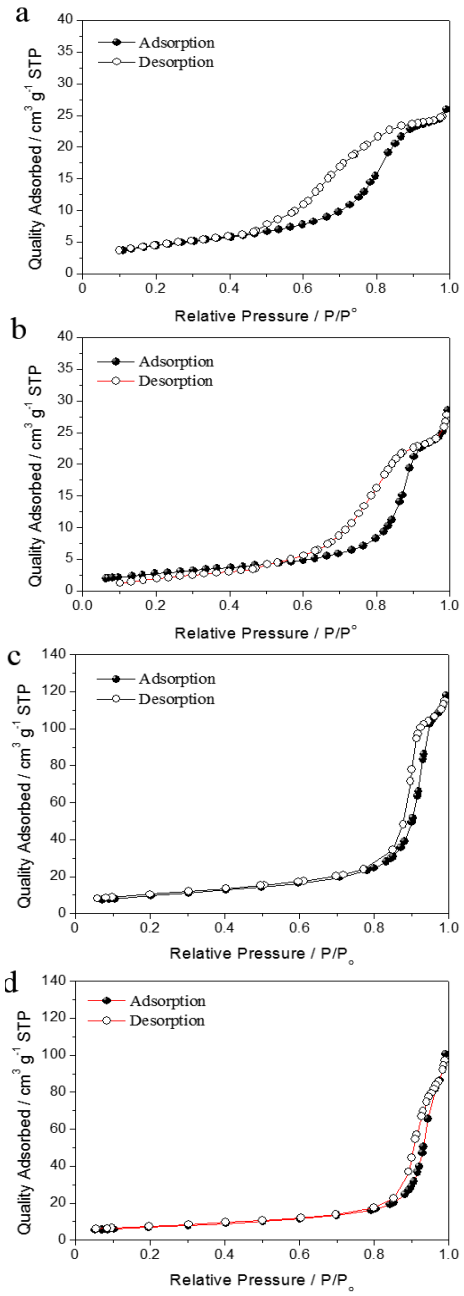

Fig. 4. N_2 adsorption-desorption isotherm of (a) ZrO_2, (b) Ag/ZrO_2, (c) TiO_2 and (d) Ag/TiO_2 nanofibers.

The crystalline structure of the TiO_2 was investigated using of X-ray diffraction (XRD) analysis and the XRD patterns TiO_2 fiber in the range of 20 to 80° is presented in Fig. 3b. The diffraction peaks (black line) showed (101), (103), (004), (112), (200), (105), (211), (213), (116), (220) and (107) planes, indicating the formation of anatase phase of titanium oxide (JCPDS No. 84-1286). The crystallite size was calculated using the Scherrer equation (1). The crystallite size of TiO_2 was 19.5 nm. This value was much smaller than that of TiO_2 fiber diameters, indicating that the fibers were composed of the crystallites of anatase phases.

Figures 4 and 5 show the N_2 adsorption -desorption isotherms and the BJH pore size distributions obtained from the desorption branch of the isotherms for TiO_2 fibers. The N_2 adsorption-desorption isotherm also confirmed that TiO_2 and Ag/TiO_2 fibers also showed type III isotherms and H3 hysteresis loops, corresponding to a mesoporous structure, as shown in Fig. 4c and d. One major pore-size peak was observed for the TiO_2 fibers at about 10.5 nm with range from 2 to 12 nm, indicating the presence of mesopores (see Fig. 5b). The pore size distribution was not so much affected by Ag deposition, whereas the pore volume was lowered due to the pore blocking by the Ag deposition and lowered amount of TiO_2 fibers contained in the catalyst. Thus, the

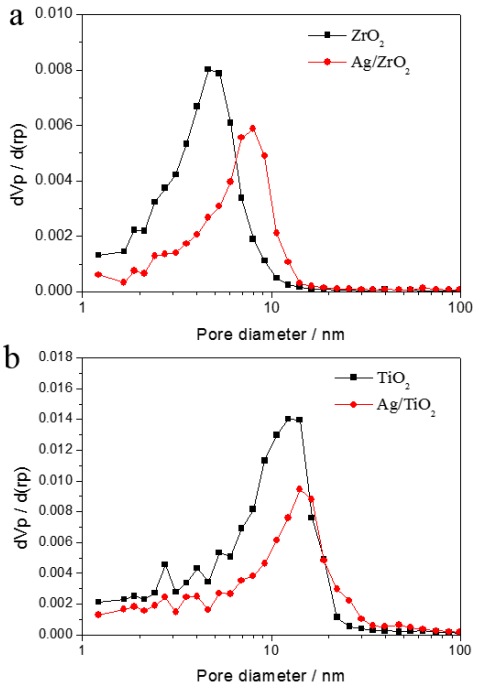

Fig. 5. BJH pore size distributions of (a) ZrO_2 and Ag/ZrO_2 and (c) TiO_2 and (d) Ag/TiO_2 nanofibers.

calcination of TiO_2 in the presence of $AgNO_3$ did not change the pore sizes, although the volume of mesopore decreased. This is in marked contrast with the results for Ag/ZrO_2.

According to the N_2 adsorption isotherms, the surface areas of the fibers were determined by the BET method. The surface areas of TiO_2 and Ag/TiO_2 fibers were calculated at 34.4 $m^2 g^{-1}$ and 24.1 $m^2 g^{-1}$, respectively. Therefore, the surface area of the fiber catalyst also decreased by the Ag deposition, which were located in the mesopores of the TiO_2 fibers blocking the pores and reduced the amount of fibers contained in the catalyst.

3.3 Comparison of ZrO_2 and TiO_2 nanofibers

As described above, the ZrO_2 and TiO_2 fiber materials prepared by the electrospinning method have both mesopores. The mesopores in the range of 2-10 nm with the maximum of 5 nm were located on the ZrO_2 fibers, whereas those in the range of 5-20 nm with the maximum of 10 nm were formed in the TiO_2 fibers. Because the mesopores were originated from the aggregation of the crystallites of ZrO_2 and TiO_2, the difference in the mesopore sizes were due to the sizes of these crystallites. As the crystallites consisting the fibers increased, the interstitial spaces, the mesopores of the fibers, which were formed by the aggregation of the crystallites increased. These findings also imply that the changes in crystalline sizes can control the mesoporous structures.

The ZrO_2 and TiO_2 fibers showed different average diameters of 105 and 240 nm, respectively. This difference can be attributed to the difference in the electrospinning parameters such as precursor solution concentration, feeding rate, spinneret inner size and applied voltage for the formation of low lever diameter (100-300 nm), which control the structures of fiber materials. On the other hand, the macroporous structures of ZrO_2 and TiO_2 fiber materials, which were originated from the interspaces formed by the nanofibers were not so much different for these two fibers. It is likely, however, that the interspace sizes can be controlled by changing the density of the nanofibers, which is also affected by the preparation conditions for fiber materials.

It is noteworthy that the post-treatment of the fiber materials changed the porous structures of the ZrO_2 fibers. When the Ag particles were deposited on the ZrO_2 fibers, the pore sizes of Ag/ZrO_2 nanofibers apparently increased. One of the explanations for this behavior is that the calcination of ZrO_2 in the presence of $AgNO_3$ promoted the sintering and coarsening of the ZrO_2 crystallites, leading to the increase in mesopores formed by the aggregation of the crystallites.

4. Summary and Conclusion

In this paper, we showed that the ZrO_2 and TiO_2 fiber materials were successfully prepared by the electrospinning method, followed by calcination at 600 and 500ºC, respectively. Both the ZrO_2 and TiO_2 fibers have the mesoporous and macroporous structures. The former structures were originated from the aggregation of crystallites. The latter structures were due to the interspace of the fibers. These fiber materials are good candidates for catalytic processes in which the adsorption, diffusion, and the morphology strongly affect the catalytic performances.

Acknowledgments

This work was partly supported by the Grant-in-Aid for Encouragement of Young Researchers of the Faculty of Engineering Sciences, Kyushu University.

References

1) Brian L. Cushing, Vladimir L. Kolesnichenko, Charles J. O'Connor, Chem. Rev. 104 (2004,) 3893−3946
2) F. E. Kruis, H. Fissan, A. Peled, J Aero. Sci, 29 (1998) 511–535
3) A. Corma, Chem. Rev. 97 (1997) 2373−2419
4) M. P. Kapoor, Y. Ichihashi, W. Shen, Y. Matsumura, Catal. Lett. 76 (2001) 139-142
5) D. Chen, F. Huang, Y. Cheng, R. A. Caruso, Adv. Mater. 21 (2009) 2206–2210
6) C. Burger, B.S. Hsiao, B. Chu, Annu. Rev. Mater. Res. 36 (2006) 333–368.
7) D.H. Reneker, I. Chun, Nanotechnology 7 (1996) 216.
8) D. Li, Y. Xia, Nano Lett. 3 (2003) 555.
9) W. Li, C.T. Laurencin, E.J. Caterson, R.S. Tuan, F.K. Ko, J. Biomed. Mater. Res. 60 (2001) 613–621.
10) D. Li, Y. Xia, Adv. Mater. 16 (2004) 1151–1170.
11) X.H. Qin, S.Y. Wang, J. Appl. Polym. Sci. 102 (2006) 1285–1290.
12) T.J. Sill, H.A. von Recum, Biomaterials. 29 (2008) 1989–2006.
13) B.C. Kim, K.S. Yang, M. Kojima, K. Yoshida, Y.J. Kim, Y.A. Kim, Adv. Funct. Mater. 16 (2006) 2393–2397.
14) S. Chuangchote, T. Sagawa, S. Yoshikawa, Appl. Phys. Lett. 93 (2008).
15) C. Lee, S. Jo, J. Choi, K.-Y. Baek, Y. Truong, I. Kyratzis, et al., J. Mater. Sci. 48 (2013) 3665–3671.
16) C. Lee, J.-I. Park, Y.-G. Shul, H. Einaga, Y. Teraoka, Appl. Catal. B Environ. 174-175 (2015) 185–192.